scientific reports

Check for updates

OPEN

Tacrolimus modulates the PI3K AKT mTOR pathway in retinal epithelial cells under inflammatory stress

Aleksandra Kiełbasińska[1,2]✉, Beniamin Oskar Grabarek[3,4], Dominika Janiszewska-Bil[2,3,5], Martyna Machaj[2,5], Zuzanna Lelek[2,5], Anita Lyssek Boroń[2,3], Michael Janusz Koss[6,7,8], Jacek Waszak[3] & Katarzyna Krysik[2,5]

Human retinal pigment epithelial (H-RPE) cells contribute to the pathogenesis of proliferative vitreoretinopathy (PVR) by undergoing inflammatory activation and fibrotic transformation. The PI3K/AKT/mTOR signaling pathway plays a central role in this process, integrating extracellular cues that promote survival, proliferation, and matrix remodeling. Tacrolimus, a calcineurin inhibitor with emerging antifibrotic properties, may modulate these responses at both transcriptional and post-transcriptional levels. H-RPE cells were treated with lipopolysaccharide (LPS), tacrolimus, or their combination to simulate inflammatory and immunosuppressive conditions. Transcriptomic profiling was performed using microarrays, followed by RT-qPCR and ELISA validation of selected targets. A parallel analysis of microRNAs (miRNAs) was conducted to assess potential regulatory interactions. Protein–protein interaction (PPI) networks were generated using the STRING database. Microarray analysis identified 38 PI3K/AKT/mTOR-associated mRNAs with significant differential expression (|FC| > 4.0, $p < 0.05$), including CDK2, PIK3CA, STAT3, MTOR, and COL1A1. LPS treatment led to strong upregulation of inflammatory and fibrotic genes, while tacrolimus reversed or attenuated many of these effects. miRNA profiling revealed inverse regulation of several transcripts by hsa-miR-27a-5p, miR-29a-3p, and miR-1271-5p. Protein measurements confirmed these trends, and STRING analysis highlighted a densely connected network with central nodes including JAK1, EGFR, and MTOR. This study supports the therapeutic potential of tacrolimus in retinal fibrosis by demonstrating its ability to modulate the PI3K/AKT/mTOR–miRNA axis in inflamed H-RPE cells, suppress key fibrotic and proliferative genes, and restore regulatory microRNA expression, offering a promising strategy for controlling H-RPE-driven remodeling PVR.

Keywords H-RPE cells, PI3K/AKT/mTOR pathway, Tacrolimus, Retinal fibrosis, PVR, Epithelial-mesenchymal transition

Abbreviations

ACTB	Actin beta
AKT	Protein kinase B
ANOVA	Analysis of variance
BDNF	Brain-derived neurotrophic factor
COL1A1	Collagen type I alpha 1 chain
COL1A2	Collagen type I alpha 2 chain
COL6A2/3	Collagen type VI alpha 2/3 chain

[1]Department of Opthalmology, University Clinical Center named after Prof. K. Gibiński of the Medical University of Silesia in Katowice, 40-514 Katowice, Poland. [2]Department of Ophthalmology, Faculty of Medicine, Academy of Silesia, 40- 555 Katowice, Poland. [3]Collegium Medicum, WSB University, 41-300 Dabrowa Gornicza, Poland. [4]Faculty of Medicine and Health Sciences, Andrzej Frycz Modrzewski University, 30-705 Cracow, Poland. [5]Department of Ophthalmology, St. Barbara Hospital, Trauma Centre, 41- 200 Sosnowiec, Poland. [6]Augenzentrum Nymphenburger Höfe, 80335 Munich, Germany. [7]Department of Ophthalmology, Augenklinik der Universität Heidelberg, 69120 Heidelberg, Germany. [8]Augenklinik Herzog Carl Theodor, 80335 Munich, Germany. ✉email: aleksandrakielbasinska96@gmail.com

CDK2/4	Cyclin-dependent kinase 2/4
EGFR	Epidermal growth factor receptor
ELISA	Enzyme-linked immunosorbent assay
EMT	Epithelial-to-mesenchymal transition
FC	Fold change
FBS	Fetal bovine serum
FGF-B	Fibroblast growth factor-basic
FZD5	Frizzled class receptor 5
GAPDH	Glyceraldehyde-3-phosphate dehydrogenase
H-RPE	Human retinal pigment epithelial (cells)
IL2/IL-6	Interleukin 2/6
IL6R	Interleukin 6 receptor
JAK1/3	Janus Kinase 1/3
KEGG	Kyoto Encyclopedia of Genes and Genomes
LPS	Lipopolysaccharide
MAP2K2 (MEK2)	Mitogen-activated protein kinase kinase 2
MAPK	Mitogen-activated protein kinase
miRNA	MicroRNA
MTOR	Mechanistic target of rapamycin
NFAT	Nuclear factor of activated T-cells
PI3K	Phosphoinositide 3-kinase
PIK3CA/B/C/D/G	Catalytic subunits alpha/beta/delta/gamma of PI3K
PPI	Protein–protein interaction
PRK	Photorefractive keratectomy (contextual assumption; not explicitly used in this manuscript)
PVR	Proliferative vitreoretinopathy
qPCR (RT-qPCR)	Quantitative real-time polymerase chain reaction
RHOA	Ras Homolog Family Member A
RNA	Ribonucleic acid
RtEBM™	Retinal pigment epithelial basal medium
SD	Standard deviation
STAT3	Signal transducer and activator of transcription 3
STRING	Search tool for the retrieval of interacting genes/proteins
TLR2/4	Toll-like receptor 2/4
TGF-β	Transforming growth factor beta
WNT1/4	Wnt Family Member 1/4

Human retinal pigment epithelial (H-RPE) cells form a polarized monolayer that is essential for retinal integrity and visual function. In addition to their classical roles in nutrient transport, phagocytosis of photoreceptor outer segments, and secretion of trophic factors, H-RPE cells function as immune-competent cells that respond dynamically to oxidative, inflammatory, and mechanical stressors[1–3]. Under pathological conditions, these cells may undergo phenotypic transformation, contributing to the development of retinal fibrotic disorders. One such disorder is proliferative vitreoretinopathy (PVR)—a serious complication of retinal detachment and vitreoretinal surgery, characterized by the formation of fibrocellular membranes on both retinal surfaces. These membranes, largely composed of transdifferentiated H-RPE cells, exert contractile forces that result in tractional retinal detachment and treatment failure[4,5]. The molecular mechanisms underlying PVR involve a combination of epithelial–mesenchymal transition (EMT), inflammation, extracellular matrix remodeling, and uncontrolled cellular proliferation—all processes driven by dysregulated intracellular signaling pathways[6–8].

Among potential therapeutic agents, tacrolimus (FK506)—a macrolide immunosuppressant traditionally used in transplant medicine—has gained attention for its pleiotropic effects on non-immune cells. By binding to FKBP12 and inhibiting calcineurin, tacrolimus prevents NFAT dephosphorylation and T-cell activation[9,10]. Beyond immune modulation, tacrolimus also influences pathways implicated in fibrosis and cell survival, including MAPK[9,11] and PI3K/AKT/mTOR[12,13], suggesting potential for repurposing in ocular fibrosis. The PI3K/AKT/mTOR signaling axis plays a central role in regulating cellular survival, proliferation, autophagy, and metabolism[14]. In H-RPE cells, activation of this pathway promotes migration, resistance to apoptosis, and ECM production—features characteristic of cells undergoing fibrotic transformation in PVR[11–13]. Importantly, PI3K/AKT/mTOR interacts with other signaling cascades, including MAPKs, to regulate inflammatory and fibrotic responses. Therefore, modulation of this pathway could represent a key therapeutic strategy in halting or reversing the cellular events that drive PVR progression[15].

In parallel, accumulating evidence highlights the role of microRNAs (miRNAs) as post-transcriptional regulators of both PI3K/AKT/mTOR and MAPK signaling. These small non-coding RNAs fine-tune gene expression by directing mRNAs toward degradation or translational repression[16]. Dysregulation of miRNAs has emerged as a key epigenetic mechanism influencing RPE cell behavior under pathological conditions[17]. In fibrotic retinal diseases such as PVR, altered miRNA expression has been linked to EMT, chronic inflammation, extracellular matrix remodeling, and enhanced proliferation[18]. By modulating the activity of key intracellular signaling pathways—including PI3K/AKT/mTOR and MAPK—miRNAs serve as integrators of environmental cues and intracellular responses, ultimately shaping disease progression[19]. Furthermore, the miRNA landscape is highly sensitive to pharmacological interventions, positioning miRNAs not only as potential biomarkers of disease activity, but also as mediators and targets of drug action[17,20].

Therefore, the aim of this study was to comprehensively evaluate the effects of tacrolimus on the gene expression profile and miRNAs-mediated regulation of the PI3K/AKT/mTOR signaling axis in H-RPE cells.

Methods

This section of the manuscript was developed based on our previously published researches[17,21].

Study design

This study investigated how tacrolimus modulates gene and microRNA expression related to the PI3K/AKT/mTOR signaling pathway in H-RPE cells under inflammatory stress. To model inflammation, cells were stimulated with lipopolysaccharide (LPS, 1 µg/mL). Four experimental groups were established: (i) untreated control, (ii) LPS alone for 6 h, (iii) tacrolimus alone (10 ng/mL) for 6, 12, or 24 h, and (iv) sequential treatment with LPS (1 µg/mL, 6 h) followed by tacrolimus (10 ng/mL) for 6, 12, or 24 h. Concentrations and incubation times were chosen based on our previous viability studies[17,21] and supporting literature[22–24].

Gene expression alterations under these conditions were evaluated using high-density oligonucleotide microarrays (HG-U133_A2, Affymetrix, Santa Clara, CA, USA), while changes in microRNA profiles were profiled using the GeneChip™ miRNA 2.0 array (Affymetrix, Santa Clara, CA, USA). A predictive mRNA–miRNA interaction analysis was conducted to identify regulatory microRNAs potentially involved in modulating the expression of differentially expressed transcripts within the PI3K/AKT/mTOR pathway. Subsequently, for selected mRNAs that consistently distinguished the LPS-stimulated cultures from those treated with LPS followed by tacrolimus—regardless of drug incubation time—protein concentration levels were quantified using enzyme-linked immunosorbent assay (ELISA). Additionally, cytotoxicity assays were performed to confirm that the applied concentrations and exposure times of LPS and tacrolimus were non-toxic and suitable for downstream molecular analyses.

Cell culture and cytotoxicity assay

Primary H-RPE cells (catalog no. 194987; Clonetics, San Diego, CA, USA) were seeded at a density of 1×10^4 cells/cm² in 25 cm² Nunclon™-treated flasks (Nunc, Wiesbaden, Germany) and cultured in retinal pigment epithelial basal medium (RtEBM™, Lonza, Basel, Switzerland) supplemented with basic fibroblast growth factor (FGF-B) and 2% fetal bovine serum (FBS). Cells were maintained in a humidified incubator (37 °C, 5% CO_2) and passaged at 80–90% confluency to preserve monolayer integrity and epithelial characteristics. For experiments, cells were grown to confluence to ensure a mature monolayer before treatment.

Cell viability following LPS and tacrolimus treatment was assessed using the MTT assay. H-RPE cells were exposed to LPS (1–10 µg/mL) or tacrolimus (0.1–100 ng/mL) for 6–24 h. At the end of the treatment period (not during), MTT reagent (0.5 mg/mL; Sigma-Aldrich, Poznań, Poland) was added and incubated for 4 h at 37 °C. The resulting formazan crystals were solubilized in DMSO, and absorbance was measured at 580 nm with a reference wavelength of 720 nm. Cell viability was calculated relative to untreated controls (100%). Detailed viability results were reported in our previous publications[17,21].

Extraction of the total ribonucleic acid (RNA)

Total RNA was extracted from cultured H-RPE cells using TRIzol reagent (Invitrogen Life Technologies, Carlsbad, CA, USA; Cat. No. 15596026), strictly following the manufacturer's protocol. To improve RNA purity and remove residual organic contaminants or salts, an additional purification step was performed using the RNeasy Mini Kit (QIAGEN, Hilden, Germany; Cat. No. 74104). To prevent genomic DNA contamination, all RNA samples underwent on-column DNase I digestion (Fermentas, Burlington, ON, Canada; Cat. No. 18047019).

The integrity of isolated RNA was evaluated by electrophoresis on a 1% agarose gel containing ethidium bromide (0.5 mg/mL), allowing for the visualization of ribosomal RNA bands. RNA concentration and purity were determined spectrophotometrically by measuring absorbance at 260 nm, ensuring suitability for downstream applications.

Microarray analysis of mRNA and MicroRNA expression

To assess how tacrolimus influences PI3K/AKT/mTOR-associated gene expression in inflammatory conditions, a high-throughput transcriptome profiling was conducted using the Affymetrix HG-U133_A2 microarray platform (Affymetrix, Santa Clara, CA, USA) and the GeneChip™ 3′ IVT PLUS Reagent Kit (Cat. No. 902416). H-RPE cells were exposed to LPS, tacrolimus, or both, and compared with untreated controls. A curated list of genes associated with the PI3K/AKT/mTOR signaling pathways was generated based on pathway annotations retrieved from the Kyoto Encyclopedia of Genes and Genomes (KEGG) via the PathCards integrative database (hsa04151 and hsa04150; accessed June 19, 2025) is reproduced with permission from Kanehisa Laboratories (Ref: 25295)[25–27]. Double-stranded cDNA was synthesized and amplified via in vitro transcription, followed by RNA fragmentation and hybridization to the microarray chips. Signal detection was carried out using the Gene Array Scanner 3000 7G and data were analyzed through the GeneChip® Command Console® Software. This methodology enabled comprehensive characterization of the transcriptional landscape associated with PI3K/AKT/mTOR signaling under experimental conditions.

To complement the mRNA analysis and explore potential post-transcriptional regulatory mechanisms, miRNA profiling was performed using the GeneChip™ miRNA 2.0 Array (Affymetrix, Santa Clara, CA, USA). The manufacturer's protocol was followed rigorously to ensure reproducibility and data integrity. Bioinformatic analysis of differentially expressed miRNAs was carried out using the TargetScan[28] and miRanda prediction tools[29], identifying putative mRNA targets involved in PI3K/AKT/mTOR signaling. Interaction scores above 90

were considered robust indicators of functional miRNA–mRNA relationships, while those below 60 were noted as low-confidence candidates pending further validation[29,30].

Reverse transcription quantitative polymerase chain reaction (RT-qPCR) validation

Relative expression levels were calculated using the $2^{-\Delta\Delta Ct}$ method. Two housekeeping genes, β-actin (*ACTB*) and glyceraldehyde-3-phosphate dehydrogenase (*GAPDH*), were used as internal controls for normalization. Primer sequences for all analyzed genes are listed in Table 1. RT-qPCR was performed with the following thermal cycling conditions: reverse transcription at 45 °C for 10 min, initial denaturation at 95 °C for 2 min, followed by 40 amplification cycles of denaturation at 95 °C for 5 s, annealing at 60 °C for 10 s, and extension at 72 °C for 5 s.

ELISA assay

The subsequent phase of molecular analysis focused on assessing protein-level changes corresponding to the genes identified during transcriptomic profiling. Protein concentrations were measured using enzyme-linked immunosorbent assay (ELISA), following the specific protocols provided by the manufacturer for each kit. The following ELISA kits, all obtained from MyBioSource (San Diego, CA, USA), were employed in the study: Human MAP2K2 ELISA Kit (catalog no MBS0331134); Human COL1A1 ELISA Kit (catalog no. MBS703198); Human COL1A2 ELISA Kit (catalog no. MBS036858); Human mTOR ELISA Kit (catalog no. MBS2505637); and Human Interleukin-2 (IL2) ELISA Kit (catalog no. MBS2020180).

Statistical analysis

All statistical analyses were conducted using the Transcriptome Analysis Console (TAC; Thermo Fisher Scientific, USA) and StatPlus software, applied uniformly across microarray, RT-qPCR, and ELISA datasets. Each experimental condition included three independent biological replicates ($n = 3$). Prior to performing comparative analyses, data distribution was assessed using the Shapiro–Wilk test to evaluate normality; datasets with p-values > 0.05 were analyzed using parametric statistical methods. One-way analysis of variance (ANOVA) was employed to assess overall differences among treatment groups. When significant effects were identified ($p < 0.05$), Scheffé's post hoc test was applied to determine specific group differences, offering stringent control of Type I error. Additionally, key pairwise comparisons (e.g., LPS vs. control, tacrolimus vs. control) were evaluated using independent-samples Student's t-tests.

For microarray data, differential gene expression was analyzed in TAC using an ANOVA-based model with a significance threshold of |fold change| > 4.0 and a Benjamini–Hochberg-adjusted p-value < 0.05 to correct for multiple testing. Venn diagrams were used to visualize overlapping and condition-specific expression changes across different exposure durations (6, 12, and 24 h). For RT-qPCR data, relative expression was calculated using the $2^{-\Delta\Delta Ct}$ method, with *ACTB* and *GAPDH* as internal reference genes. To account for variability, results were expressed as mean RQ values accompanied by RQmin and RQmax intervals derived from ΔCt variance. Statistical significance was determined using one-way ANOVA with Scheffé's post hoc test.

For ELISA-based protein quantification, concentrations were calculated from standard curves and presented as mean ± SD. Intergroup differences across treatments and time points were assessed using two-way ANOVA (treatment × time interaction), with Bonferroni correction applied for multiple comparisons where appropriate. To explore functional gene interactions, protein–protein interaction (PPI) enrichment analysis was conducted using the STRING database (v11.0). Interaction significance was assessed by comparing the observed PPI network to a randomly generated network of equal size. The enrichment strength was expressed as Log_{10}(observed/expected), and false discovery rate (FDR)-adjusted p-values were calculated to account for multiple comparisons[31].

mRNA	Starter	Sequence
IL-2	Forward	5'-TCCTCAACTCCTGCCACAATG-3'
	Reverse	5'-TGTGAGCATCCTGGTGAGTT-3'
MTOR	Forward	5'-CCTGCCTTTGTCATGCCTTT-3'
	Reverse	5'-CTGGGTTTGGATCAGGGTCT-3'
MAP2K2	Forward	5'-GGGACGTTCATCACCAACAC-3'
	Reverse	5'-CTTCAGGTAGTACAGCGCCT-3'
COL1A1	Forward	5'- GCTACTACCGGGCTGATGAT-3'
	Reverse	5'- ACCAGTCTCCATGTTGCAGA-3'
COL1A2	Forward	5'- GAGAGAGCGGTAACAAGGGT-3'
	Reverse	5'- GAAGACCACGAGAACCAGGA-3'
ACTB	Forward	5'-TCACCCACACTGTGCCCATCTACGA-3'
	Reverse	5'-CAGCGGAACCGCTCATTGCCAATGG-3'
GAPDH	Forward	5'- GGTGAAGGTCGGAGTCAACGGA-3'
	Reverse	5'- GAGGGATCTCGCTCCTGGAAGA-3'

Table 1. Primers sequences used to RT-qPCR. IL2, interleukin 2; MTOR, Mechanistic Target of Rapamycin; MAP2K2, Mitogen-Activated Protein Kinase Kinase 2; COL1A1, Collagen Type I Alpha 1 Chain; COL1A2, Collagen Type I Alpha 2 Chain; ACTB, Actin Beta; GAPDH, Glyceraldehyde-3-Phosphate Dehydrogenase

Results

Impact of inflammatory and immunosuppressive stimuli on H-RPE viability assessed by MTT assay

As previously detailed in our earlier descriptions[17], the MTT assay results demonstrated that exposure of H-RPE cells to 1 µg/mL of LPS did not produce a statistically significant impact on cell viability ($p = 0.784$). However, higher concentrations of LPS (2 and 10 µg/mL) led to a significant reduction in viability over time, particularly when comparing the 6-hour mark with later time points ($p = 0.023$ and $p = 0.022$, respectively). These findings point to a dose- and time-dependent cytotoxic effect at elevated LPS levels.

In contrast, tacrolimus at the lowest tested concentration (0.1 ng/mL) induced statistically significant viability changes between 6 and 12 h and between 12 and 24 h ($p = 0.0027$), indicating a time-sensitive cellular response. Interestingly, higher doses of tacrolimus (1 to 100 ng/mL) did not yield statistically significant fluctuations in viability, suggesting that cytotoxic effects may not escalate linearly with dose in this range. When LPS (1 µg/mL) and tacrolimus (10 ng/mL) were combined, the reduction in viability approached significance ($p = 0.0786$) but remained borderline.

Taking these findings into account, together with our previously published MTT viability data[17] and prior studies[10,22,32–35], concentrations of 1 µg/mL LPS and 10 ng/mL tacrolimus were chosen for downstream experiments, as they allowed for biological activity without compromising cell viability.

Microarray analysis identified 38 differentially expressed PI3K/AKT/mTOR-related mRNAs

From the 469 PI3K/AKT/mTOR-associated mRNAs curated from KEGG, ANOVA initially identified 43 transcripts with significant differential expression ($|FC| > 4.0$, $p < 0.05$). A post hoc test refined this set to 38 robustly differentially expressed genes (DEGs) across treatment conditions. Specifically, in H-RPE cells exposed to tacrolimus for 6 h (H_6 vs. C), 18 DEGs were identified, of which 8 were unique to this time point. At 12 h (H_{12} vs. C), 9 DEGs were observed, including 3 that were time-point-specific. At 24 h (H_{24} vs. C), 12 DEGs were found, with 3 unique to this interval. In addition, 5 mRNAs were consistently regulated across all time points. Thus, the final count of 38 DEGs represents the overlap and refined output of the ANOVA and post hoc analyses (Fig. 1).

In turn, Table 2 shows the changes in the expression pattern of the selected 38 mRNAs $p < 0.05$). Microarray analysis revealed that exposure of H-RPE cells to LPS (H6) led to a robust upregulation of multiple genes associated with the PI3K/AKT/mTOR pathway, including *CDK2*, *CDK4*, *PIK3CA–D*, *JAK1*, *JAK3*, *STAT3*, *EGFR*, *MAP2K2*, and collagen genes (*COL6A2*, *COL6A3*, *COL1A1*, *COL1A2*), indicating enhanced cell proliferation, matrix remodeling, and inflammatory signaling. Tacrolimus alone induced a suppressive effect on many of these targets, notably downregulating *CDK2*, *CDK4*, *PIK3CB–D*, *STAT3*, and *TLRs*, while paradoxically increasing *IL-6* and *IL-2* expression. Combined treatment (LPS + tacrolimus) produced a biphasic response, with initial downregulation of key PI3K/AKT/mTOR components at H6 (including *PIK3CA*, *STAT3*, *EGFR*, and *MTOR*), followed by partial reactivation at H12–H24, particularly among *JAK1*, *JAK3*, *IL-2*, and *BDNF*, suggesting a compensatory pro-inflammatory shift. Notably, matrix-related genes and WNT pathway members remained suppressed under combination treatment at later time points, indicating sustained inhibition of fibrotic signaling (Table 2; $p < 0.05$).

RT-qPCR validated differential expression of selected mRNAs

RT-qPCR confirmed the microarray data. *IL-2* expression was significantly increased following tacrolimus treatment (RQ = 4.6, RQmin–RQmax = 3.9–5.4) and in LPS + Tacrolimus groups at 6 h (RQ = 3.5, 2.8–4.3), 12 h (RQ = 5.9, 5.1–6.7), and 24 h (RQ = 4.2, 3.5–5.0). By contrast, *MTOR* expression was suppressed, with values ranging from RQ = 0.19 (0.15–0.23) at 6 h to RQ = 0.23 (0.18–0.29) at 24 h. *MAP2K2* was downregulated across all time points (e.g., 6 h: RQ = 0.12, 0.09–0.16; 24 h: RQ = 0.07, 0.05–0.09). Similarly, *COL1A1* (RQ = 0.09–0.21) and COL1A2 (RQ = 0.11–0.33) exhibited marked reductions under LPS + Tacrolimus conditions. The distribution of replicate values for each condition is shown in Fig. 2, while the corresponding quantitative summary (RQ with RQmin–RQmax) is provided in Table S1 (Supplementary Material) (Fig. 2).

Distinct MicroRNA signatures regulate IL-2, MTOR, and COL1A1 in LPS- and tacrolimus-treated H-RPE cells

The integrated mRNA–miRNA expression analysis revealed distinct regulatory interactions between selected transcripts and their targeting microRNAs in H-RPE cells (Table 3; $p < 0.05$). IL-2 mRNA expression increased significantly under LPS stimulation (log_2FC up to + 3.89 ± 0.43), coinciding with a marked downregulation of its predicted regulatory miRNAs: hsa-miR-462 (–2.19 ± 0.51), miR-27a-5p (–3.29 ± 0.42), and miR-3163 (–2.34 ± 0.43), indicating inverse regulation. Similarly, MTOR was strongly induced under LPS + tacrolimus treatment (log_2FC up to + 3.76 ± 0.91), while miR-3182 and miR-1271-5p were initially suppressed under LPS (log_2FC up from–2.87 to − 3.09) and subsequently upregulated by tacrolimus. COL1A1 expression was elevated following co-treatment, accompanied by a prior decrease and later recovery of miR-29a-3p, a known anti-fibrotic miRNA (LPS: − 3.98 ± 0.87; LPS + tacrolimus H24: +2.91 ± 0.34).

ELISA quantification of PI3K/AKT/mTOR-related proteins in H-RPE cells

The analysis of protein concentrations in H-RPE cell cultures revealed distinct, treatment- and time-dependent changes across all examined targets (Table 4; $p < 0.05$). LPS stimulation significantly increased the levels of MAP2K2, COL1A1, COL1A2, and MTOR, with peak concentrations observed at 6–12 h post-treatment. In contrast, tacrolimus alone moderately reduced MAP2K2, COL1A1, COL1A2, and MTOR levels relative to LPS but remained higher than control in most cases. Combined treatment with LPS and tacrolimus resulted in a marked and progressive reduction of these protein levels over time, falling below both LPS and control levels

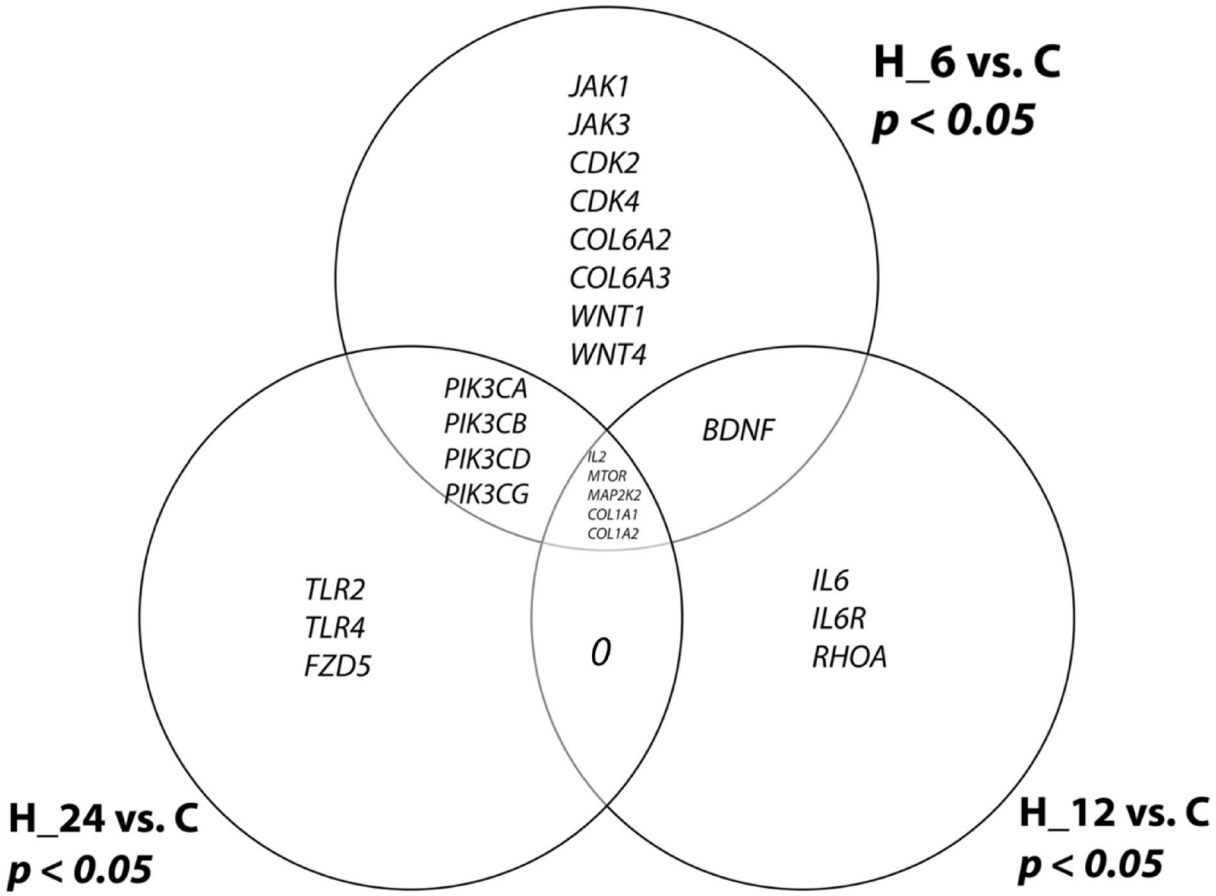

Fig. 1. Venn diagram illustrating the overlap and time-specific distribution of differentially expressed mRNAs (|FC| > 4.0, $p < 0.05$) associated with the PI3K/AKT/mTOR signaling pathway in LPS-treated H-RPE cells following tacrolimus exposure. H_6, H_12, and H_24 indicate cells harvested after 6, 12, and 24 h of tacrolimus treatment, respectively; C represents untreated control cells. Genes abbreviation: CDK2, Cyclin-Dependent Kinase 2; CDK4, Cyclin-Dependent Kinase 4; COL6A2, Collagen Type VI Alpha 2 Chain; COL6A3, Collagen Type VI Alpha 3 Chain; WNT1, Wnt Family Member 1; WNT4, Wnt Family Member 4; JAK1, Janus Kinase 1; JAK3, Janus Kinase 3; STAT3, Signal Transducer and Activator of Transcription 3; EGFR, Epidermal Growth Factor Receptor; PIK3CA, Phosphatidylinositol-4,5-Bisphosphate 3-Kinase Catalytic Subunit Alpha; PIK3CB, Phosphatidylinositol-4,5-Bisphosphate 3-Kinase Catalytic Subunit Beta; PIK3CD, Phosphatidylinositol-4,5-Bisphosphate 3-Kinase Catalytic Subunit Delta; PIK3CG, Phosphatidylinositol-4,5-Bisphosphate 3-Kinase Catalytic Subunit Gamma; IL-6, Interleukin 6; IL6R, Interleukin 6 Receptor; RHOA, Ras Homolog Family Member A; TLR2, Toll-Like Receptor 2; TLR4, Toll-Like Receptor 4; FZD5, Frizzled Class Receptor 5; IL-2, Interleukin 2; MTOR, Mechanistic Target of Rapamycin Kinase; MAP2K2, Mitogen-Activated Protein Kinase Kinase 2; COL1A1, Collagen Type I Alpha 1 Chain; COL1A2, Collagen Type I Alpha 2 Chain; BDNF, Brain-Derived Neurotrophic Factor.

by 24 h. IL-2 showed a distinct pattern, with its concentration progressively increasing under all treatment conditions, most notably after combined exposure, reaching the highest value at 12 h (34.98 ± 3.43 pg/mL).

Network analysis identifies interconnected PI3K/AKT/mTOR signaling modules

The STRING network analysis of the 26 PI3K/AKT/mTOR pathway-associated genes reveals a highly interconnected protein-protein interaction (PPI) network with 139 observed edges, significantly exceeding the expected number of 51 interactions for a random network of this size. The average node degree of 10.7 and a high local clustering coefficient of 0.767 indicate a densely clustered and functionally cohesive interaction landscape. The PPI enrichment p-value of < 1.0e-16 confirms that the proteins are significantly more connected than expected by chance, suggesting strong biological interrelationships. Central hubs include JAK1, STAT3, IL6, EGFR, MTOR, and PIK3CA, which bridge inflammatory, proliferative, and survival signaling. Peripheral clusters represent collagens (COL1A1/2, COL6A2/3) and WNT components (WNT1, WNT4, FZD5), linked to extracellular matrix remodeling and epithelial-mesenchymal transition (Fig. 3).

Probeset ID	mRNA	LPS	Tacrolimus	LPS + tacrolimus		
		log_2 fold change				
		H_6 vs. C	H_6 vs. C	H_6 vs. C	H_12 vs. C	H_24 vs. C
204252_at	*CDK2*	+ 4.34	-2.75	+ 4.13	+ 2.81	+ 2.99
211803_at		+ 4.32	-2.87	+ 4.32	+ 2.91	+ 3.12
211804_s_at		+ 4.16	-3.10	+ 4.18	+ 2.77	+ 2.76
202246_s_at	*CDK4*	+ 3.47	-3.45	+ 4.98	+ 4.12	+ 3.11
209156_s_at	*COL6A2*	+ 4.56	+ 2.11	+ 2.87	-3.34	-4.48
213290_at		+ 4.61	+ 2.81	+ 2.98	-3.31	-4.77
201438_at	*COL6A3*	+ 4.16	+ 2.98	-3.24	-4.01	-4.12
208570_at	*WNT1*	+ 2.98	+ 1.98	-5.43	-2.34	-2.37
208606_s_at	*WNT4*	+ 3.12	+ 2.34	-4.32	-2.34	-2.34
230751_at		+ 3.45	+ 2.81	-4.56	-2.65	-2.87
1556689_a_at		+ 2.91	+ 2.09	-4.91	-2.98	-2.17
201648_at	*JAK1*	+ 3.45	+ 3.21	+ 3.44	-2.99	+ 5.45
239695_at		+ 3.21	+ 3.32	+ 3.42	-3.21	+ 4.98
240613_at		+ 3.61	+ 3.09	+ 3.56	-3.12	+ 5.61
1552610_a_at		+ 3.71	+ 3.81	+ 4.01	-2.76	+ 5.43
1552611_a_at		+ 3.63	+ 315	+ 3.87	-2.81	+ 5.87
207187_at	*JAK3*	+ 2.54	+ 3.18	+ 3.98	+ 4.85	+ 5.63
211108_s_at		+ 2.61	+ 2.99	+ 4.14	+ 5.12	+ 5.76
211109_at		+ 2.83	+ 3.65	+ 4.16	+ 4.91	+ 6.01
227677_at		+ 2.81	+ 3.61	+ 3.99	+ 4.98	+ 5.43
208991_at	*STAT3*	+ 3.41	+ 2.12	-3.45	-4.11	-4.09
208992_s_at		+ 3.71	+ 2.87	-3.71	-4.32	-4.32
225289_at		+ 3.18	+ 2.51	-3.56	-4.87	-4.51
		+ 3.65	+ 2.71	-3.81	-4.23	-4.74
201983_s_at	*EGFR*	+ 4.17	+ 1.19	-2.34	-4.56	-4.32
201984_s_at		+ 4.51	+ 1.87	-2.65	-4.32	-4.76
210984_x_at		+ 4.32	+ 1.34	-2.43	-4.61	-4.89
211550_at		+ 4.55	+ 1.44	-2.71	-5.12	-4.71
211551_at		+ 4.16	+ 1.11	-2.45	-4.78	-4.88
211607_x_at		+ 4.71	+ 1.16	-2.55	-4.34	-4.91
224999_at		+ 4.61	+ 1.21	-2.87	-4.54	-4.76
1565483_at		+ 4.74	+ 1.19	-2.19	-4.43	-4.53
1565484_x_at		+ 4.18	+ 1.16	-2.97	-4.67	-4.71
204369_at	*PIK3CA*	+ 5.67	+ 2.65	-5.60	-5.87	-5.12
231854_at		+ 5.93	+ 2.51	-5.17	-5.43	-5.43
235980_at		+ 5.44	+ 2.76	-5.87	-5.67	-5.61
212688_at	*PIK3CB*	+ 5.42	-3.45	-4.13	-4.35	-4.78
217620_s_at		+ 5.76	-3.16	-4.61	-4.86	-4.56
203879_at	*PIK3CD*	+ 4.17	-3.18	-5.67	-4.12	-4.91
211230_s_at		+ 4.51	-3.71	-6.19	-4.25	-5.02
206369_s_at	*PIK3CG*	+ 4.98	-2.11	-3.87	-4.51	-4.65
206370_at		+ 5.17	-2.23	-4.15	-4.16	-4.77
205207_at	*IL-6*	-3.12	+ 5.13	+ 5.23	+ 4.62	-3.17
205945_at	*IL6R*	+ 3.71	-2.25	-4.87	-4.12	-3.31
217489_s_at		+ 3.17	-2.17	-5.41	-4.41	-3.45
226333_at		+ 4.01	-2.65	-4.81	-4.22	-3.41
200059_s_at	*RHOA*	+ 2.13	-1.56	-4.12	-3.54	-3.12
240337_at		+ 2.35	-1.61	-4.65	-3.67	-2.76
1555814_a_at		+ 2.81	-1.74	-4.87	-3.61	-3.45
204924_at	*TLR2*	+ 6.17	-2.34	-4.56	-5.43	-5.21
221060_s_at	*TLR4*	+ 5.45	-2.13	-5.43	-5.66	-4.87
224341_x_at		+ 5.17	-2.17	-5.43	-5.62	-4.56
232068_s_at		+ 5.74	-2.32	-4.98	-5.44	-4.99
1552798_a_at		+ 5.26	-2.01	-5.23	-5.87	-4.72

Continued

Probeset ID	mRNA	LPS	Tacrolimus	LPS + tacrolimus		
		$\log_2$ fold change				
		H_6 vs. C	H_6 vs. C	H_6 vs. C	H_12 vs. C	H_24 vs. C
206136_at	*FZD5*	+ 3.42	+ 1.98	-4.01	-3.45	-2.12
221245_s_at		+ 3.16	+ 2.01	-3.46	-4.01	-2.13
207849_at	*IL-2*	+ 1.11	+ 4.17	+ 3.69	+ 5.41	+ 4.12
202288_at	*MTOR*	+ 2.11	+ 2.01	-4.17	-2.21	-1.87
215381_at		+ 2.76	+ 2.13	-4.32	-2.34	-2.01
202424_at	*MAP2K2*	+ 4.98	+ 2.18	-3.49	-4.99	-4.32
213487_at		+ 4.61	+ 2.13	-3.76	-4.12	-4.56
213490_s_at		+ 5.18	+ 2.34	-3.81	-5.16	-4.61
202310_s_at	*COL1A1*	+ 4.71	+ 2.18	-4.32	-4.19	-3.41
202311_s_at		+ 4.51	+ 2.16	-4.56	-4.52	-3.54
202312_s_at		+ 4.99	+ 2.56	-4.23	-4.87	-3.66
217430_x_at		+ 4.16	+ 2.61	-4.71	-4.68	-3.18
1556499_s_at		+ 4.64	+ 2.47	-4.41	-4.17	-3.81
202403_s_at	*COL1A2*	+ 5.67	+ 1.98	-4.11	-3.87	-2.18
202404_s_at		+ 5.81	+ 2.17	-4.32	-3.91	-2.12
229218_at		+ 5.17	+ 2.03	-4.87	-4.01	-2.81
206382_s_at	*BDNF*	+ 2.34	+ 2.89	+ 4.51	+ 4.09	+ 2.12
239367_at		+ 2.12	+ 2.99	+ 4.44	+ 4.13	+ 2.34

Table 2. Microarray profile of PI3K/AKT/mTOR signaling pathway–dependent genes in H-RPE cultures exposed to LPS, tacrolimus, or their combination (|FC| > 4.00 in any comparison; all listed mRNAs are statistically significant, $p < 0.05$). Data are presented as mean ± SD; (+), overexpression compared to the control; (−), downregulated compared to the control; C, control culture; H_6, H_12, H_24 refer to cultures exposed to LPS, tacrolimus, or their combination for 6, 12, and 24 h, respectively; LPS, lipopolysaccharide. *CDK2*, Cyclin-Dependent Kinase 2; *CDK4*, Cyclin-Dependent Kinase 4; *COL6A2*, Collagen Type VI Alpha 2 Chain; *COL6A3*, Collagen Type VI Alpha 3 Chain; *WNT1*, Wnt Family Member 1; *WNT4*, Wnt Family Member 4; *JAK1*, Janus Kinase 1; *JAK3*, Janus Kinase 3; *STAT3*, Signal Transducer and Activator of Transcription 3; *EGFR*, Epidermal Growth Factor Receptor; *PIK3CA*, Phosphatidylinositol-4,5-Bisphosphate 3-Kinase Catalytic Subunit Alpha; *PIK3CB*, Phosphatidylinositol-4,5-Bisphosphate 3-Kinase Catalytic Subunit Beta; *PIK3CD*, Phosphatidylinositol-4,5-Bisphosphate 3-Kinase Catalytic Subunit Delta; *PIK3CG*, Phosphatidylinositol-4,5-Bisphosphate 3-Kinase Catalytic Subunit Gamma; *IL-6*, Interleukin 6; *IL6R*, Interleukin 6 Receptor; *RHOA*, Ras Homolog Family Member A; *TLR2*, Toll-Like Receptor 2; *TLR4*, Toll-Like Receptor 4; *FZD5*, Frizzled Class Receptor 5; *IL-2*, Interleukin 2; *MTOR*, Mechanistic Target of Rapamycin Kinase; *MAP2K2*, Mitogen-Activated Protein Kinase Kinase 2; *COL1A1*, Collagen Type I Alpha 1 Chain; *COL1A2*, Collagen Type I Alpha 2 Chain; *BDNF*, Brain-Derived Neurotrophic Facto

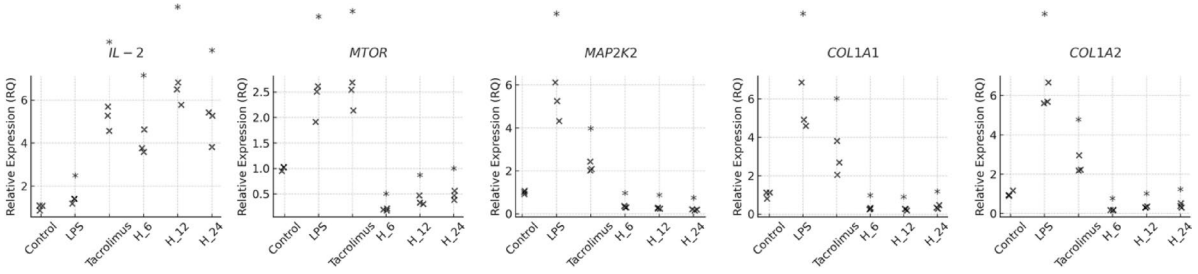

Fig. 2. RT-qPCR validation of PI3K/AKT/mTOR-related mRNAs. Dot plots show relative expression (RQ = $2^{-\Delta\Delta Ct}$) of *IL-2*, *MTOR*, *MAP2K2*, *COL1A1*, and *COL1A2* in H-RPE cells treated with LPS, tacrolimus, or their combination for 6 h, 12 h, and 24 h compared with control (C). Each dot represents one biological replicate ($n = 3$). Asterisks denote significant differences compared to control ($p < 0.05$). Genes abbreviation: *IL-2*, Interleukin 2; *MTOR*, Mechanistic Target of Rapamycin Kinase; *MAP2K2*, Mitogen-Activated Protein Kinase Kinase 2; *COL1A1*, Collagen Type I Alpha 1 Chain; *COL1A2*, Collagen Type I Alpha 2 Chain.

mRNA	miRNA	Target score	LPS	Tacrolimus	LPS + tacrolimus		
			log_2 fold change				
			H_6 vs. C	H_6 vs. C	H_6 vs. C	H_12 vs. C	H_24 vs. C
IL-2	hsa-miR-462	98	-2.19 ± 0.51	2.65 ± 0.34	3.17 ± 0.54	3.76 ± 0.22	3.89 ± 0.43
	hsa-miR-27a-5p	94	-3.29 ± 0.42	3.14 ± 0.31	2.78 ± 0.76	3.54 ± 0.34	4.01 ± 0.45
	hsa-miR-3163	90	-2.34 ± 0.43	2.87 ± 0.19	2.98 ± 0.71	2.89 ± 0.42	3.01 ± 0.16
MTOR	hsa-miR-3182	92	-2.87 ± 0.18	1.54 ± 0.81	3.45 ± 0.4	3.76 ± 0.91	3.18 ± 0.76
	hsa-miR-1271-5p	97	-3.09 ± 0.33	2.01 ± 0.23	4.56 ± 0.65	3.76 ± 0.17	3.11 ± 0.12
COL1A1	hsa-miR-29a-3p	98	-3.98 ± 0.87	-1.01 ± 0.19	2.34 ± 0.81	2.76 ± 0.43	2.91 ± 0.34
COL1A2		90					

Table 3. Differential expression of selected mRNAs and their regulatory MicroRNAs in H-RPE cells treated with LPS or LPS with tacrolimus compared to Control. Data are presented as mean ± SD. *IL-2*, Interleukin 2; *MTOR*, Mechanistic Target of Rapamycin Kinase; *MAP2K2*, Mitogen-Activated Protein Kinase Kinase 2; *COL1A1*, Collagen Type I Alpha 1 Chain; *COL1A2*, Collagen Type I Alpha 2 Chain; LPS, ipopolysaccharide; C, control cell culture; FC, fold change; C: control culture; H_6, H_8, and H_24, time of exposure to the medicine. All listed changes are statistically significant compared to control (C) ($p < 0.05$).

Protein	C	LPS	Tacrolimus	LPS + tacrolimus		
				H_6	H_12	H_24
MAP2K2 [ng/mL]	1.55 ± 0.11	2.87 ± 0.12	1.99 ± 0.17	0.96 ± 0.08	0.76 ± 0.22	0.72 ± 0.12
COL1A1 [ng/mL]	10.98 ± 0.32	12.45 ± 0.23	7.87 ± 0.54	4.12 ± 0.43	2.84 ± 0.43	1.77 ± 0.18
COL1A2 [ng/mL]	21.53 ± 0.98	28.98 ± 1.23	20.11 ± 0.91	6.87 ± 0.66	6.55 ± 0.32	4.65 ± 0.43
MTOR [ng/mL]	2.60 ± 0.12	5.76 ± 0.17	3.11 ± 0.32	1.76 ± 0.77	1.11 ± 0.71	1.09 ± 0.23
IL-2 [pg/mL]	14.87 ± 1.32	23.87 ± 1.34	24.89 ± 2.34	28.90 ± 2.31	34.98 ± 3.43	32.82 ± 2.09

Table 4. Time-Dependent changes in the concentration of selected proteins in H-RPE cell cultures treated with LPS, Tacrolimus, or their combination compared to Control. Data are presented as mean ± SD IL-2, Interleukin 2; MTOR, Mechanistic Target of Rapamycin Kinase; MAP2K2, Mitogen-Activated Protein Kinase Kinase 2; COL1A1, Collagen Type I Alpha 1 Chain; COL1A2, Collagen Type I Alpha 2 Chain; LPS, lipopolisaccharide A; C, control cell culture; FC, fold change; C: control culture; H_6, H_8, and H_24, time of exposure to the medicine All listed changes are statistically significant compared to control (C) ($p < 0.05$).

Discussion

Retinal detachment compromises the structural integrity of the posterior segment, enabling RPE cells to migrate into the vitreous cavity. In this pro-inflammatory microenvironment—rich in cytokines and growth factors—RPE cells encounter mitogenic and immunoregulatory cues that drive sustained activation and promote proliferative vitreoretinopathy (PVR)[2,36]. Several cell types, particularly RPE-derived myofibroblasts, fibroblasts, macrophages, and astrocytes, contribute to pathological remodeling by enhancing proliferation, migration, and extracellular matrix (ECM) deposition, ultimately leading to recurrent detachment and vision loss[37,38]. The high concentrations of cytokines and growth factors detected in vitreous samples from PVR patients support the "growth factor and cytokine hypothesis," implicating dysregulated signaling in chronic retinal fibrosis[39,40].

In this study, tacrolimus exerted a time-dependent effect on gene expression in inflamed human RPE cells (H-RPE). The number of differentially expressed genes decreased over time, likely reflecting reduced intracellular drug activity through CYP3A4/3A5 metabolism or subcellular sequestration[41,42].

These pharmacokinetic dynamics highlight the importance of optimized delivery strategies—such as sustained-release formulations—to maintain therapeutic concentrations in chronic fibrotic conditions. The 10 ng/mL tacrolimus dose used was confirmed as non-toxic, ensuring that observed transcriptional changes reflected pharmacological activity rather than cytotoxicity. Transcriptomic profiling confirmed that LPS induces a pro-fibrotic and pro-inflammatory shift in PI3K/AKT/mTOR-associated genes. Among 469 curated pathway members, 38 were differentially expressed, with five genes—*IL-2*, *MTOR*, *MAP2K2*, *COL1A1*, and *COL1A2*—showing consistent regulation under tacrolimus treatment. These were selected for in-depth validation.

Tacrolimus suppressed LPS-induced upregulation of *COL1A1* and *COL1A2*, encoding type I collagen chains, the main structural components of fibrotic epiretinal membranes in PVR. Suppression was observed at both mRNA and protein levels and accompanied by re-expression of miR-29a-3p, a known inhibitor of ECM genes[43,44]. miR-29 family downregulation is a hallmark of fibrosis across multiple organs[45–47], and its restoration can reduce collagen deposition and myofibroblast transdifferentiation[48–51].

In ocular tissues, miR-29a-3p protects against excessive ECM accumulation[43,44]. This suggests that tacrolimus may help restore antifibrotic homeostasis through two complementary mechanisms: by directly repressing profibrotic transcriptional programs and by promoting miRNA-mediated silencing pathways.

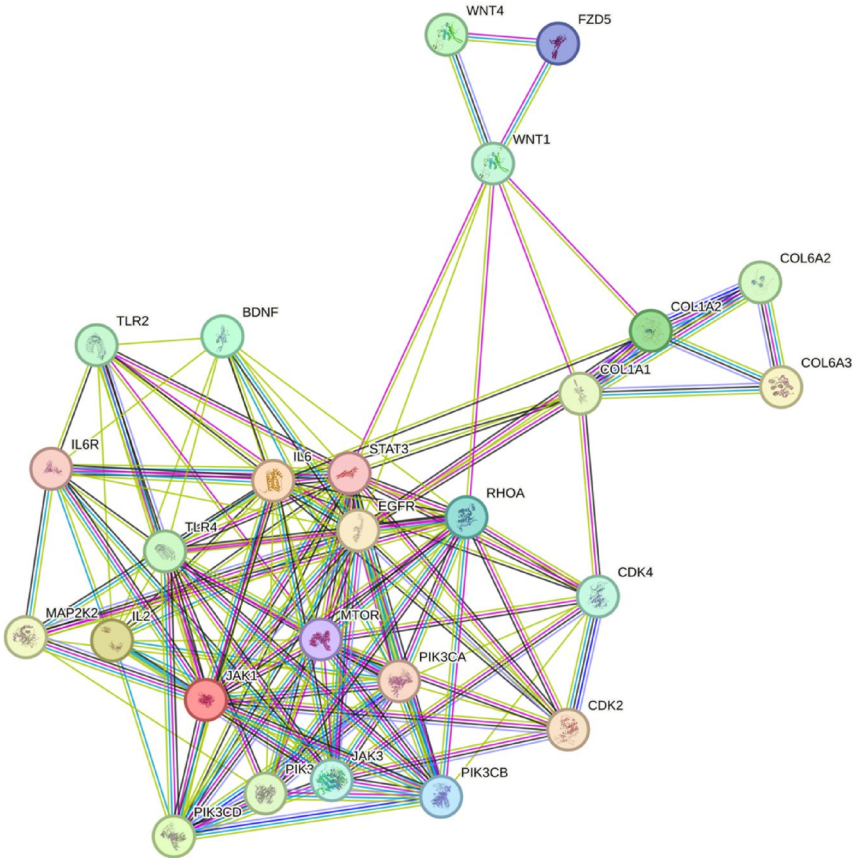

Fig. 3. Protein interaction network for PI3K/AKT/MTOR signaling pathway differentiation-related genes generated using the STRING database.

MTOR, a master regulator of growth, metabolism, and survival, was also suppressed at transcript and protein levels. This effect coincided with upregulation of miR-1271-5p and miR-3182, both predicted MTOR regulators. Hyperactivation of MTOR promotes EMT and ECM accumulation in H-RPE[52–54], while inhibition reduces fibroproliferation[55–59]. Therefore, tacrolimus suppression of MTOR, partly through miRNA regulation, may underlie its antifibrotic potential.

MAP2K2 (MEK2) was downregulated at transcript and protein levels. Although no miRNA regulators were confirmed, suppression of MEK2 suggests indirect targeting of MAPK signaling, potentially contributing to reduced proliferation under inflammatory stress[60,61].

In contrast, IL-2 was consistently upregulated by tacrolimus. While tacrolimus normally inhibits IL-2 in T cells via calcineurin[60,61].

Previous studies in immortalized ARPE-19 cells demonstrated that IL-2 can stimulate extracellular matrix synthesis and promote TGF-β2 expression, thereby contributing to pro-fibrotic phenotypes[62]. However, ARPE-19 cells are known to differ substantially from native human RPE, both morphologically and at the molecular level. For instance, comparative analyses have shown that ARPE-19 exhibit altered senescence, stress responses, and gene expression profiles relative to primary or iPSC-derived H-RPE, suggesting they represent an immature phenotype[63]. In contrast, the present study was conducted in primary H-RPE cells, which more closely recapitulate in vivo physiology. Thus, while IL-2 upregulation observed here may signal a potential fibrotic risk, translation of ARPE-19 findings to H-RPE should be made with care, and additional in vivo investigations will be required to clarify whether tacrolimus-induced IL-2 expression results in functional fibrotic changes in the retinal microenvironment.

Low-level IL-2 signaling has also been reported to stabilize T regulatory (Treg) cells, promoting immune resolution[64,65]. The incomplete restoration of IL-2-targeting miRNAs (miR-27a-5p, miR-462, miR-3163) in our model may explain its sustained upregulation. Clinically, modest IL-2 induction could enhance immune quiescence, debris clearance, or remodeling[66,67].

However, given that IL-2 can independently promote fibrosis[68], its upregulation remains a potential liability and warrants in vivo validation before therapeutic translation.

Our STRING network analysis of 26 differentially expressed PI3K/AKT/mTOR-related genes revealed a densely interconnected system with 139 observed edges, far exceeding the 51 expected for a random network of similar size ($p < 1.0e-16$). This connectivity underscores the central role of PI3K/AKT/mTOR signaling in coordinating proliferation, metabolism, survival, and immune responses, all of which are dysregulated in PVR. Central hubs included JAK1, STAT3, IL6, EGFR, MTOR, and PIK3CA, which integrate inflammatory,

fibrotic, and survival cues. The JAK1–STAT3–IL6 axis is a well-established driver of cytokine-mediated H-RPE activation and epithelial-mesenchymal transition (EMT)[69,70], while EGFR and PIK3CA function upstream of AKT/mTOR to promote proliferation and metabolic reprogramming[71,72]. Peripheral modules enriched for collagen genes (COL1A1, COL1A2, COL6A2, COL6A3) and WNT signaling components (WNT1, WNT4, FZD5) reflect downstream shifts toward ECM deposition and EMT, consistent with collagen-rich membranes and RPE transdifferentiation in PVR[73,74]. The co-occurrence of WNT1, WNT4, and FZD5 with collagen genes highlights a mechanotransduction link, as WNT signaling is tightly associated with ECM stiffness, turnover, and scarring, processes that amplify RPE plasticity and contractile remodeling[75,76]. Inclusion of TLR2 and TLR4 further emphasizes the anchoring role of innate immune activation in initiating this cascade[75,76].

Importantly, tacrolimus did not act as a passive inhibitor of this network but dynamically reshaped it by downregulating profibrotic and proliferative signals (MTOR, MAP2K2, COL1A1/2) while selectively preserving or enhancing immune-related functions (IL-2, JAK/STAT). This context-specific modulation suggests a dual role: suppressing fibrosis while maintaining reparative or immunoregulatory responses[77]. Clinically, such network-level effects may enable therapeutic strategies that limit fibrotic progression in PVR without inducing global immunosuppression, thereby reducing risks such as opportunistic infection or impaired regeneration[17]. The identified molecular nodes and sub-networks also provide a roadmap for combinatory approaches, such as pairing tacrolimus with antifibrotic miRNA mimics (e.g., miR-29a-3p) or sustained-release intraocular formulations[78,79].

This study has limitations. The use of immortalized HRPE-19 cells in vitro cannot fully recapitulate the in vivo retinal environment with its complex cell–matrix and immune interactions. Validation was limited to a subset of proteins, and additional assays (e.g., Western blotting, immunocytochemistry, phosphoproteomics) would strengthen mechanistic conclusions. Predicted miRNA–mRNA interactions were not directly confirmed with reporter assays. Finally, the analysis focused on early transcriptional and post-transcriptional responses (6–24 h), whereas long-term pharmacodynamics and in vivo effects remain to be clarified.

Future work should include in vivo PVR models to validate identified targets, investigate tacrolimus pharmacokinetics and retention in ocular tissues, and explore combined therapies with miRNA mimics or antifibrotic small molecules. The observed differential regulation of IL-2 and collagen suggests selective immune modulation, with potential implications not only for PVR but also for other fibrotic ocular diseases such as AMD-associated subretinal fibrosis or fibrotic uveitis. Advanced methods such as phosphoproteomics or single-cell transcriptomics could further dissect tacrolimus-induced signaling rewiring under inflammatory stress.

Conclusion

In conclusion, our findings demonstrate that tacrolimus modulates key components of the PI3K/AKT/mTOR signaling pathway in inflamed RPE cells, exerting selective antifibrotic and immunomodulatory effects relevant to the pathogenesis of proliferative vitreoretinopathy. The consistent downregulation of fibrotic effectors such as COL1A1, COL1A2, MTOR, and MAP2K2, alongside the paradoxical upregulation of IL-2, highlights tacrolimus's capacity to reshape cellular behavior in a context-dependent manner. Notably, the associated regulation of microRNAs—including miR-29a-3p, miR-1271-5p, miR-3182, and miR-27a-5p—suggests that miRNA-mediated post-transcriptional control plays a central role in mediating these effects. These findings not only reinforce the therapeutic promise of tacrolimus in retinal fibrosis but also point to miRNAs as potential co-targets or biomarkers in future precision treatment strategies for PVR and related retinal disorders.

Data availability

The data that support the findings of this study are available from the corresponding author upon reasonable request.

Received: 1 July 2025; Accepted: 16 September 2025
Published online: 21 October 2025

References

1. Lakkaraju, A. et al. The cell biology of the retinal pigment epithelium. *Prog. Retin. Eye Res.* **78**, 100846. https://doi.org/10.1016/j.preteyeres.2020.100846 (2020).
2. Gupta, S. et al. Retinal pigment epithelium cell development: extrapolating basic biology to stem cell research. *Biomedicines* **11**, 310. https://doi.org/10.3390/biomedicines11020310 (2023).
3. Yang, S., Zhou, J. & Li, D. Functions and diseases of the retinal pigment epithelium. *Front. Pharmacol.* **12**, 727870 (2021).
4. Ferro Desideri, L., Artemiev, D., Zandi, S., Zinkernagel, M. S. & Anguita, R. Proliferative vitreoretinopathy: An update on the current and emerging treatment options. *Graefes Arch. Clin. Exp. Ophthalmol.* **262**, 679–687. https://doi.org/10.1007/s00417-023-06264-1 (2024).
5. Assi, A. & Charteris, D. Proliferative vitreoretinopathy: A revised concept of retinal injury and response. *Br. J. Ophthalmol.* **108**, 1621–1626. https://doi.org/10.1136/bjo-2023-324417 (2024).
6. Harju, N., Kauppinen, A. & Loukovaara, S. Fibrotic changes in rhegmatogenous retinal detachment. *Int. J. Mol. Sci.* **26**, 1025. https://doi.org/10.3390/ijms26031025 (2025).
7. Szczepan, M., Llorián-Salvador, M., Chen, M. & Xu, H. Immune cells in subretinal wound healing and fibrosis. *Front. Cell. Neurosci.* **16**, 916719. https://doi.org/10.3389/fncel.2022.916719 (2022).
8. Zhu, C., Cheng, Y., Tang, Y. & Wu, H. Changes of aqueous humor cytokine profiles of patients with high intraocular pressure after PPV for retinal detachment (2023).
9. Wang, M., Zhou, J., Niu, Q. & Wang, H. Mechanism of tacrolimus in the treatment of lupus nephritis. *Front. Pharmacol.* **15**, 1331800 (2024).
10. Rebibo, L. et al. Topical tacrolimus nanocapsules eye drops for therapeutic effect enhancement in both anterior and posterior ocular inflammation models. *J. Control Release* **333**, 283–297. https://doi.org/10.1016/j.jconrel.2021.03.035 (2021).

11. Aa, A., Ha, O., Fem, F. H. & Amm, A. Impact of the ACE2 activator Xanthenone on tacrolimus nephrotoxicity: Modulation of uric acid/ERK/p38 MAPK and Nrf2/SOD3/GCLC signaling pathways. *Life Sci.*. https://doi.org/10.1016/j.lfs.2021.120154 (2022).
12. Yu, L., Wei, J. & Liu, P. Attacking the PI3K/Akt/mTOR signaling pathway for targeted therapeutic treatment in human cancer. *Sem. Cancer Biol.* **85**, 69–94. https://doi.org/10.1016/j.semcancer.2021.06.019 (2022).
13. Chen, X., Hu, K., Zhang, Y., He, S-M. & Wang, D-D. Targeting CXCR2 ameliorated tacrolimus-induced nephrotoxicity by alleviating overactivation of PI3K/AKT/mTOR pathway and calcium overload. *Biomed. Pharmacother.* **180**, 117526. https://doi.org/10.1016/j.biopha.2024.117526 (2024).
14. Huang, J. et al. Targeting the PI3K/AKT/mTOR signaling pathway in the treatment of human diseases: Current status, trends, and solutions. *J. Med. Chem.* **65**, 16033–16061. https://doi.org/10.1021/acs.jmedchem.2c01070 (2022).
15. Stefani, C. et al. PI3K/AKT/mTOR and MAPK signaling pathways in colorectal cancer pathogenesis: Where are we now? *Int. J. Mol. Sci.* **22**, 10260. https://doi.org/10.3390/ijms221910260 (2021).
16. Amoushahi, M., Jørgensen, P. H., Kjeldgaard, A. B., Padi, E. & Fossum, M. MicroRNAs and hypospadias: A systematic review. *Med. Int.* **5**, 7. https://doi.org/10.3892/mi.2024.206 (2025).
17. Kiełbasińska, A. et al. Tacrolimus modulates TGF-β Signaling-Related genes and MicroRNAs in human retinal pigment epithelial cells activated by lipopolysaccharide. *Int. J. Mol. Sci.* **26**, 5402. https://doi.org/10.3390/ijms26115402 (2025).
18. Yao, Q., Chen, Y. & Zhou, X. The roles of MicroRNAs in epigenetic regulation. *Curr. Opin. Chem. Biol.* **51**, 11–17. https://doi.org/10.1016/j.cbpa.2019.01.024 (2019).
19. MicroRNAs' role in the environment-related non-communicable diseases and link to multidrug resistance, regulation, or alteration - PubMed n.d. https://pubmed.ncbi.nlm.nih.gov/34046834/. Accessed 17 June 2025.
20. Artesunate inhibits the development. of PVR by suppressing the TGF-β/Smad signaling pathway - PubMed n.d.. https://pubmed.ncbi.nlm.nih.gov/34822854/. Accessed 17 June 2025.
21. Kiełbasińska, A. et al. Evaluation of gene expression and the regulatory role of MicroRNAs related to the Mitogen-Activated protein kinase signaling pathway in human retinal pigment epithelial cells treated with lipopolysaccharide A and tacrolimus. *Mediators Inflamm.* **2025**, 8586711. https://doi.org/10.1155/mi/8586711 (2025).
22. Kimsa, M. et al. Transforming growth factor β-related genes in human retinal pigment epithelial cells after tacrolimus treatment. *Pharmacol. Rep.* **68**, 969–974. https://doi.org/10.1016/j.pharep.2016.04.020 (2016).
23. Qiu, R. et al. The protective effects of VVN001 on LPS-Induced inflammatory responses in human RPE cells and in a mouse model of EIU. *Inflammation* **44**, 780–794. https://doi.org/10.1007/s10753-020-01377-9 (2021).
24. Klettner, A. & Roider, J. Retinal pigment epithelium expressed toll-like receptors and their potential role in age-related macular degeneration. *Int. J. Mol. Sci.* **22**, 8387 (2021).
25. Kanehisa, M., Furumichi, M., Sato, Y., Kawashima, M. & Ishiguro-Watanabe, M. KEGG for taxonomy-based analysis of pathways and genomes. *Nucleic Acids Res.* **51**, D587–D592. https://doi.org/10.1093/nar/gkac963 (2023).
26. Kanehisa, M., Furumichi, M., Sato, Y., Matsuura, Y. & Ishiguro-Watanabe, M. KEGG: Biological systems database as a model of the real world. *Nucleic Acids Res.* **53**, D672–D677. https://doi.org/10.1093/nar/gkae909 (2025).
27. Kanehisa, M. & Goto, S. KEGG: Kyoto encyclopedia of genes and genomes. *Nucleic Acids Res.* **28**, 27–30. https://doi.org/10.1093/nar/28.1.27 (2000).
28. Agarwal, V., Bell, G. W., Nam, J-W. & Bartel, D. P. Predicting effective MicroRNA target sites in mammalian mRNAs. *eLife* **4**, e05005. https://doi.org/10.7554/eLife.05005 (2015).
29. Chen, Y. & Wang, X. MiRDB: An online database for prediction of functional MicroRNA targets. *Nucleic Acids Res.* **48**, D127–D131. https://doi.org/10.1093/nar/gkz757 (2020).
30. Liu, W. & Wang, X. Prediction of functional MicroRNA targets by integrative modeling of MicroRNA binding and target expression data. *Genome Biol.* **20**, 18. https://doi.org/10.1186/s13059-019-1629-z (2019).
31. Szklarczyk, D. et al. The STRING database in 2023: Protein-protein association networks and functional enrichment analyses for any sequenced genome of interest. *Nucleic Acids Res.* **51**, D638–D646. https://doi.org/10.1093/nar/gkac1000 (2023).
32. Brandli, A., Vessey, K. A. & Fletcher, E. L. The contribution of pattern recognition receptor signalling in the development of age related macular degeneration: The role of toll-like-receptors and the NLRP3-inflammasome. *J. Neuroinflamm.* **21**, 64. https://doi.org/10.1186/s12974-024-03055-1 (2024).
33. Ren, Y. et al. Effects of tacrolimus on the TGF–β1/SMAD signaling pathway in paraquat–exposed rat alveolar type II epithelial cells. *Mol. Med. Rep.* **22**, 3687–3694. https://doi.org/10.3892/mmr.2020.11453 (2020).
34. Binsaleh, A. Y. et al. Tacrolimus versus hydrocortisone in management of atopic dermatitis in children, a randomized controlled double-blind study: New insights on TARC, CTACK, TSLP, and E-selectin. *Immun. Inflamm. Dis.* **12**, e70028. https://doi.org/10.1002/iid3.70028 (2024).
35. Lee, C. et al. Oxidative photocatalysis on membranes triggers non-canonical pyroptosis. *Nat. Commun.* **15**, 4025. https://doi.org/10.1038/s41467-024-47634-5 (2024).
36. George, S. M., Lu, F., Rao, M., Leach, L. L. & Gross, J. M. The retinal pigment epithelium: Development, injury responses, and regenerative potential in mammalian and non-mammalian systems. *Prog. Retin. Eye Res.* **85**, 100969 (2021).
37. Chaudhary, R. et al. Inflammatory and fibrogenic factors in proliferative vitreoretinopathy development. *Transl. Vis. Sci. Technol.* **9**, 23. https://doi.org/10.1167/tvst.9.3.23 (2020).
38. Sharma, S. et al. A simulacrum of proliferative vitreoretinopathy (PVR): Development and proteomics-based validation of an in vitro model. *J. Proteins Proteom.* **15**, 105–118. https://doi.org/10.1007/s42485-024-00140-0 (2024).
39. Dai, Y., Dai, C. & Sun, T. Inflammatory mediators of proliferative vitreoretinopathy: Hypothesis and review. *Int. Ophthalmol.* **40**, 1587–1601. https://doi.org/10.1007/s10792-020-01325-4 (2020).
40. Tsotridou, E. et al. A review of last decade developments on epiretinal membrane pathogenesis. *Med. Hypothesis Discov. Innov. Ophthalmol.* **9**, 91–110 (2020).
41. Manubolu, K. Pharmaceutical drug interactions. In *A Short Guide To Clinical Pharmacokinetics* 37–52 (eds Manubolu, K., Peeriga, R. & Chandrasekhar, K. B.) (Springer, 2024). https://doi.org/10.1007/978-981-97-4283-7_3.
42. Li, X., Zhao, M. & He, S. RPE epithelial-mesenchymal transition plays a critical role in the pathogenesis of proliferative vitreoretinopathy. *Ann. Transl. Med.* **8**, 263 (2020).
43. Huang, J. et al. Mesenchymal cell-derived exosomes and miR-29a-3p mitigate renal fibrosis and vascular rarefaction after renal ischemia reperfusion injury. *Stem Cell. Res. Ther.* **16**, 135. https://doi.org/10.1186/s13287-025-04226-4 (2025).
44. Han, S., Wang, Z., Liu, J., David Wang, H-M. & Yuan, Q. Corrigendum to miR-29a-3p-dependent COL3A1 and COL5A1 expression reduction assists sulforaphane to inhibit gastric cancer progression [Biochem. Pharmacol. 188 (2021) 114539]. *Biochem. Pharmacol.* **208**, 115389. https://doi.org/10.1016/j.bcp.2022.115389 (2023).
45. Tian, Y. et al. Immunosuppressants tacrolimus and sirolimus revert the cardiac antifibrotic properties of p38-MAPK inhibition in 3D-multicellular human iPSC-heart organoids. *Front. Cell. Dev. Biol.* **10**, 1001453. https://doi.org/10.3389/fcell.2022.1001453 (2022).
46. Wang, M. et al. The role of MiR-29 in the mechanism of fibrosis. *Mini Rev. Med. Chem.* **23**, 1846–1858. https://doi.org/10.2174/1389557523666230328125031 (2023).
47. Cushing, L. et al. miR-29 is a major regulator of genes associated with pulmonary fibrosis. *Am. J. Respir Cell. Mol. Biol.* **45**, 287–294. https://doi.org/10.1165/rcmb.2010-0323OC (2011).

48. Meyer, N., Brodowski, L., von Kaisenberg, C., Schröder-Heurich, B. & von Versen-Höynck, F. Cyclosporine A and tacrolimus induce functional impairment and inflammatory reactions in endothelial progenitor cells. *Int. J. Mol. Sci.* **22**, 9696. https://doi.org/10.3390/ijms22189696 (2021).
49. Nabavi, M. H. et al. A collagen-based hydrogel containing tacrolimus for bone tissue engineering. *Drug Deliv. Transl. Res.* **10**, 108–121. https://doi.org/10.1007/s13346-019-00666-7 (2020).
50. Wang, D., Chen, X., Fu, M., Xu, H. & Li, Z. Tacrolimus increases the expression level of the chemokine receptor CXCR2 to promote renal fibrosis progression. *Int. J. Mol. Med.* **44**, 2181–2188. https://doi.org/10.3892/ijmm.2019.4368 (2019).
51. Lee, W-S. et al. Tacrolimus regulates Endoplasmic reticulum stress-mediated osteoclastogenesis and inflammation: In vitro and collagen-induced arthritis mouse model. *Cell. Biol. Int.* **42**, 393–402. https://doi.org/10.1002/cbin.10861 (2018).
52. Shamsan, E. et al. The role of PI3k/AKT signaling pathway in attenuating liver fibrosis: A comprehensive review. *Front. Med.* **11**, 1389329. https://doi.org/10.3389/fmed.2024.1389329 (2024).
53. Yu, J. J. & Goncharova, E. A. mTOR signaling network in cell biology and human disease. *Int. J. Mol. Sci.* **23**, 16142. https://doi.org/10.3390/ijms232416142 (2022).
54. Tong, L. et al. Tacrolimus inhibits insulin release and promotes apoptosis of Min6 cells through the Inhibition of the PI3K/Akt/mTOR pathway. *Mol. Med. Rep.* **24**, 658. https://doi.org/10.3892/mmr.2021.12297 (2021).
55. Tang, Q. et al. TGF-β-induced PI3K/AKT/mTOR pathway controls myofibroblast differentiation and secretory phenotype of valvular interstitial cells through the modulation of cellular senescence in a naturally occurring in vitro canine model of myxomatous mitral valve disease. *Cell. Prolif.* **56**, e13435. https://doi.org/10.1111/cpr.13435 (2023).
56. Shigematsu, T. et al. The mTOR inhibitor everolimus attenuates tacrolimus-induced renal interstitial fibrosis in rats. *Life Sci.* **288**, 120150. https://doi.org/10.1016/j.lfs.2021.120150 (2022).
57. Moldvai, D. et al. Tumorigenic role of tacrolimus through mTORC1/C2 activation in post-transplant renal cell carcinomas. *Br. J. Cancer* **130**, 1119–1130. https://doi.org/10.1038/s41416-024-02597-8 (2024).
58. Bernard, M. & Hébert M-J. Autophagy drives fibroblast senescence through MTORC2 regulation. *Autophagy* **16**, 2004–2016. https://doi.org/10.1080/15548627.2020.1713640 (2020).
59. Wei, X., Luo, L. & Chen, J. Roles of mTOR signaling in tissue regeneration. *Cells* **8**, 1075. https://doi.org/10.3390/cells8091075 (2019).
60. Whitehouse, G. et al. IL-2 therapy restores regulatory T-cell dysfunction induced by calcineurin inhibitors. *Proc. Natl. Acad. Sci. U. S. A.* **114**, 7083–7088. https://doi.org/10.1073/pnas.1620835114 (2017).
61. Zakerkish, F., Soriano, M. J., Novella-Mestre, E., Brännström, M. & Díaz-García, C. Differential effects of the immunosuppressive calcineurin inhibitors cyclosporine-A and tacrolimus on ovulation in a murine model. *Hum. Reprod. Open* **2021**, hoab012. https://doi.org/10.1093/hropen/hoab012 (2021).
62. Jing, R. et al. Interleukin-2 induces extracellular matrix synthesis and TGF-β2 expression in retinal pigment epithelial cells. *Dev. Growth Differ.* **61**, 410–418. https://doi.org/10.1111/dgd.12630 (2019).
63. Voisin, A. et al. hRPE cells derived from induced pluripotent stem cells are more sensitive to oxidative stress than ARPE-19 cells. *Exp. Eye Res.* **177**, 76–86. https://doi.org/10.1016/j.exer.2018.07.017 (2018).
64. Nasa, Y. et al. Concomitant use of interleukin-2 and tacrolimus suppresses follicular helper T cell proportion and exerts therapeutic effect against lupus nephritis in systemic lupus erythematosus-like chronic graft versus host disease. *Front. Immunol.* **15**, 1326066. https://doi.org/10.3389/fimmu.2024.1326066 (2024).
65. Hirai, T. et al. IL-2 receptor engineering enhances regulatory T cell function suppressed by calcineurin inhibitor. *Am. J. Transpl.* **22**, 3061–3068. https://doi.org/10.1111/ajt.17181 (2022).
66. Liu, B. et al. Tacrolimus alleviates pulmonary fibrosis progression through inhibiting the activation and interaction of ILC2 and monocytes. *Int. Immunopharmacol.* **132**, 111999. https://doi.org/10.1016/j.intimp.2024.111999 (2024).
67. Lee, H., Myoung, H. & Kim, S. M. Review of two immunosuppressants: Tacrolimus and cyclosporine. *J. Korean Assoc. Oral Maxillofac. Surg.* **49**, 311–323 (2023).
68. Datta, S., Cano, M., Ebrahimi, K., Wang, L. & Handa, J. T. The impact of oxidative stress and inflammation on RPE degeneration in non-neovascular AMD. *Prog. Retin. Eye Res.* **60**, 201–218. https://doi.org/10.1016/j.preteyeres.2017.03.002 (2017).
69. Chen, X., Yang, W., Deng, X., Ye, S. & Xiao, W. Interleukin-6 promotes proliferative vitreoretinopathy by inducing epithelial-mesenchymal transition via the JAK1/STAT3 signaling pathway. *Mol. Vis.* **26**, 517–529 (2020).
70. Xiao, R., Lei, C., Zhang, Y. & Zhang, M. Interleukin-6 in retinal diseases: From pathogenesis to therapy. *Exp. Eye Res.* **233**, 109556. https://doi.org/10.1016/j.exer.2023.109556 (2023).
71. Shu, D. Y., Butcher, E. & Saint-Geniez, M. EMT and endmt: emerging roles in age-related macular degeneration. *Int. J. Mol. Sci.* **21**, 4271. https://doi.org/10.3390/ijms21124271 (2020).
72. Wang, S. et al. Reversed senescence of retinal pigment epithelial cell by coculture with embryonic stem cell via the TGFβ and PI3K pathways. *Front. Cell. Dev. Biol.* **8**, 588050. https://doi.org/10.3389/fcell.2020.588050 (2020).
73. Wang, Y. et al. Connective tissue growth factor promotes retinal pigment epithelium mesenchymal transition via the PI3K/AKT signaling pathway. *Mol. Med. Rep.* **23**, 1–13 (2021).
74. Hayat, R., Manzoor, M. & Hussain, A. Wnt signaling pathway: A comprehensive review. *Cell. Biol. Int.* **46**, 863–877. https://doi.org/10.1002/cbin.11797 (2022).
75. Kawai, T., Ikegawa, M., Ori, D. & Akira, S. Decoding Toll-like receptors: Recent insights and perspectives in innate immunity. *Immunity* **57**, 649–673. https://doi.org/10.1016/j.immuni.2024.03.004 (2024).
76. De Chiara, S. et al. Beyond the toll-like receptor 4. Structure-dependent lipopolysaccharide recognition systems: How far are we? *ChemMedChem* **20**, e202400780. https://doi.org/10.1002/cmdc.202400780 (2025).
77. Mahaparn, I. et al. The association of tacrolimus formulation on cerebral blood flow and cognitive function. *Transpl. Direct* **9**, e1511. https://doi.org/10.1097/TXD.0000000000001511 (2023).
78. Mehjabin, A. et al. MicroRNA in fibrotic disorders: A potential target for future therapeutics. *Front. Biosci.* **28**, 317. https://doi.org/10.31083/j.fbl2811317 (2023).
79. Wang, Y. et al. MiR-22-3p and miR-29a-3p synergistically inhibit hepatic stellate cell activation by targeting AKT3. *Exp. Biol. Med.* **247**, 1712–1731. https://doi.org/10.1177/15353702221108379 (2022).

Acknowledgements

The authors would like to thank Mr. Oskar Ogloszka for his valuable assistance in improving the English language of the manuscript. The authors gratefully acknowledge Kanehisa Laboratories for granting permission to use KEGG pathway images under an Open Access license (Ref: Ref: 25295).

Author contributions

A.K. is responsible for conceptualization, investigation, visualization, writing—original draft, review, and editing. K.K. is responsible for data curation and writing—original draft and final approval of the version to be published, revising it critically. D.J.B. and A.L.-B. are responsible for visualization; M.M., and Z.Z., J.W. are responsible for literature search. M.S and P.M. are responsible for statistical analysis. B.O.G. is responsible for con-

ceptualization, writing—review and editing, revising it critically, final approval of the version to be published, revising it critically and project administration. M.J.K. is responsible for writing—original draft. All authors reviewed the manuscript.

Declarations

Competing interests

The authors declare no competing interests.

Additional information

Supplementary Information The online version contains supplementary material available at https://doi.org/10.1038/s41598-025-20650-1.

Correspondence and requests for materials should be addressed to A.K.

Reprints and permissions information is available at www.nature.com/reprints.

Publisher's note Springer Nature remains neutral with regard to jurisdictional claims in published maps and institutional affiliations.